

## Article

# A Novel Online State-of-Health Estimation Method for Lithium-Ion Batteries with Multi-Input Metabolic Long Short-Term Memory Framework

Lin Chen <sup>1</sup>, Deqian Chen <sup>1,2</sup>, Manping He <sup>1</sup>, Haihong Pan <sup>1,\*</sup> and Bing Ji <sup>3,\*</sup>

<sup>1</sup> School of Mechanical Engineering, Guangxi University, Nanning 530004, China; chenlin@gxu.edu.cn (L.C.); 2111301005@st.gxu.edu.cn (D.C.); 2211393003@st.gxu.edu.cn (M.H.)

<sup>2</sup> School of Intelligent Manufacturing and Automotive Engineering, Chongqing Vocational College of Transportation, Chongqing 402247, China

<sup>3</sup> School of Engineering, University of Leicester, Leicester LE1 7RH, UK

\* Correspondence: panhhgxx@gxu.edu.cn (H.P.); bing.ji@leicester.ac.uk (B.J.)

**Abstract:** Accurate and effective battery state-of-health (SoH) monitoring is significant to guarantee the security and dependability of electrical equipment. However, adapting SoH estimation methods to diverse battery kinds and operating conditions is a challenge because of the intricate deterioration mechanisms of batteries. To solve the issue, in this article, a novel multi-input metabolic long short-term memory (MM-LSTM) framework is developed. A degradation state model is created with the LSTM network to describe the intricate deterioration mechanisms. To convey more information about battery aging, the capacity degradation, sample entropy of discharge voltage, and ohmic internal resistance increment are extracted as the inputs of the model. To estimate SoH with a few data, the metabolic mechanisms are introduced to update the inputs and reflect the latest developments in aging. The accuracy and robustness of the proposed MM-LSTM framework are verified in different aspects using two kinds of batteries, and the maximum estimation error of SoH is within 1.98%. The findings indicate that the MM-LSTM framework implements the transfer application of SoH estimate successfully, and the framework's versatility has been proven.



Received: 30 December 2024

Revised: 14 February 2025

Accepted: 18 February 2025

Published: 21 February 2025

**Citation:** Chen, L.; Chen, D.; He, M.;

Pan, H.; Ji, B. A Novel Online

State-of-Health Estimation Method for

Lithium-Ion Batteries with

Multi-Input Metabolic Long

Short-Term Memory Framework.

*Energies* **2025**, *18*, 1037. <https://doi.org/10.3390/en18051037>

**Copyright:** © 2025 by the authors.

Licensee MDPI, Basel, Switzerland.

This article is an open access article distributed under the terms and conditions of the Creative Commons Attribution (CC BY) license

(<https://creativecommons.org/licenses/by/4.0/>).

## 1. Introduction

Due to its high energy density, high stability, and extended lifespan, lithium-ion batteries are extensively used in many different types of machinery and equipment, particularly electric vehicles (EVs) [1–3]. The battery state-of-health (SoH) impacts the stability and reliability of the entire vehicle and establishes the time frame for battery replacement. The primary competency of battery management systems (BMSs) has always been the precise and robust SoH estimation [4]. In addition to maximizing battery performance, accurate online SoH estimation can increase battery safety and prevent unintentional battery failure [5]. Therefore, the creation and development of SoH estimation techniques is essential. Numerous estimation strategies have been suggested in order to provide robust and accurate SoH estimation. They are mainly separated into three groups: filter-based approaches, experimental approaches, and data-driven approaches [6].

The state space equation is mostly used in filter-based methods to estimate the characteristic parameters and afterward determine the battery SoH. Due to their superior capacity

to process non-linear data, particle filter (PF) and Kalman filter (KF) are regarded as the standard approaches [7,8]. A multi-stage PF prediction model was put up by Pan et al. [9] to address the problem of battery capacity regeneration in SoH estimation. Wu et al. [10] suggested an improved firefly algorithm to replace the re-sampling of the conventional particle filter for the combined estimate of the battery state of charge (SoC) and SoH, taking into account the particle degradation issue of the standard particle filter algorithm. Zhu et al. [11] integrated the unscented Kalman filter (UKF) and improved the unscented particle filter (IUPF) to increase the efficiency and precision of SoH estimation by dividing the 4-dimensional UPF into 3-dimensional UKF and 1-dimensional UPF. Although filter-based approaches have strengths in processing non-linear data and eliminating noise, they do not have the ability to transfer applications, and more battery test data are needed to reconstruct the model when battery operating conditions change.

By analyzing the experimental data, the experimental methods directly predict the battery's aging tendency. A popular technique is coulomb counting, which involves charging the battery completely, followed by a tiny current discharge that lasts until the battery voltage hits the cut-off point. The discharge capacity is calculated and the SoH is determined [12]. Electrochemical impedance spectroscopy (EIS) is another popular technique that estimates battery SoH by examining the connection between impedance and SoH [13]. In addition, battery aging behavior is analyzed for SoH estimate by processing measurement data, such as voltage, using incremental capacity analysis (ICA) [14] and differential voltage analysis (DVA) [15]. Although these SoH estimation techniques are quite fundamental and precise, they require specific tests and they have stringent requirements for testing environments and experimental instruments, making them unsuitable for engineering applications.

The machine learning (ML) algorithm used by the data-driven approaches, which can describe the intricate degradation process of batteries without extensive internal chemical mechanism study, predicts the degradation trend [16]. The data-driven approach uses historical data from battery operation to train the ML model for SoH estimation, which is smart and flexible and enables online estimation. As a result, it has emerged as one of the most popular subjects in battery SoH research. Support vector machine (SVM), support vector regression (SVR), Gaussian process regression (GPR), neural network (NN), and others are a few of these techniques. An SVM model was created by Feng et al. [17] to capture the peculiarities of the battery charging profile at various SoHs. The SoH was calculated based on a customized similarity function. To realize the battery SoH estimation, Yang et al. [18] used the battery discharge voltage and temperature to extract the degradation features, used the Gaussian function combined with sigmoid as the kernel function of relevance vector machine (RVM), and adopted particle swarm optimization to solve the best weight and kernel function parameters of multi-core RVM. Song et al. [19] built a SoH estimation framework using a feed-forward neural network (FFNN) by big data platform, and the effectiveness of the estimation framework was verified by monitoring 700 vehicles with different driving patterns. Wei et al. [20] developed an SVR-based SoH state-space model for batteries to describe the capacity change rule between neighboring cycles. They took representative features from the constant-voltage and constant-current protocols and used them as the model's input variables. The results demonstrated the method's ability to produce reliable and accurate results. When given enough historical data as input, data-driven approaches perform well at adapting to non-linear problems and satisfactory results can be obtained [21]. Chen et al. [22] presented a degeneration state model that utilizes an extreme learning machine (ELM). A metabolic mechanism was employed to eliminate outdated data and include the most recent data, ultimately achieving SoH estimation for the whole battery life cycle through iteration. GPR has the ability to

make accurate predictions with a small amount of data. Richardson et al. [23] proposed Gaussian process regression for in situ capacity estimation (GP-ICE), which requires only 10 s of voltage data from a constant current discharge for SoH estimation, with a root-mean-square error (RMSE) of no more than 3%. However, this method cannot be used for dynamic operating conditions. Transfer learning (TL) was introduced in 1995 to solve the problem of lifelong learning by reusing previous knowledge, which relaxes the restriction that training and test data must follow the same distribution [24]. Since TL can leverage the knowledge of one task or domain to improve the performance of another task or domain, it has become a widely adopted method in various fields. Currently, TL is widely used to solve natural language processing challenges, emotion classification problems, and image classification problems [25]. In terms of battery SOH estimation, Shu et al. [26] proposed a SoH estimation model incorporating LSTM and TL for the SoH estimation of different types of batteries, with 40% less training data without compromising the estimation performance. Tang et al. [27] developed a transferable attention neural network to simultaneously predict battery SoH and remaining useful life (RUL). Through multi-task learning, the model was able to learn the common features of the SoH and RUL prediction tasks using LSTM, and the unique features using the fully connected (FC) layer. Tan et al. [28] proposed a TL-based SoH estimation method using a small amount of data for training to obtain SoH estimates for more stages. The method used LSTM and FC as the fundamental training models and used the feature expression scoring (FES) rule to evaluate the correlation between different tasks. The task with the highest FES score was chosen for training in order to produce the best-generalized base model. These methods reduce the amount of data used for training, but still train multiple models.

In this research, a multi-input metabolic long short-term memory (MM-LSTM) model is proposed to overcome the limitations of the vast quantity of data required by traditional data-driven approaches and the requirement to train several models for transfer learning. Specifically, a degradation state model based on LSTM is developed to describe the complex degradation mechanism of batteries. The model uses capacity degradation as the state variable, and discharge voltage sample entropy and ohmic internal resistance increment as the observation variables. A metabolic mechanism is introduced to update the inputs of the model. The model is initialized with four cycles of historical data to complete the SoH estimation of the subsequent aging cycles. LSTM has superior performance in learning long-term dependencies [29,30] and is commonly used to learn common features across tasks. At the same stage, battery aging causes the battery voltage to change. Sample entropy captures the complexity and small changes in the voltage signal to convey battery aging information. The increase in internal resistance is also one of the most significant realizations of lithium-ion battery aging. The LSTM model proposed by Zhang et al. [31] obtained accurate SoH results using 20–25% of the measured data with limited data. Compared with this study, MM-LSTM only used four cycles of data to complete SoH estimation.

The important contributions made in this paper are as follows:

- (1) A multi-input metabolic long short-term memory (MM-LSTM) model is proposed, which learns the common features of battery aging, estimates battery SoH for different batteries and different operating conditions, and achieves transfer application for SoH estimation.
- (2) A metabolic mechanism is introduced to update the inputs of the LSTM-based degradation state model, which reduces the data required for the initialization of the SoH estimation and achieves the SoH estimation using a small amount of data. The metabolic mechanism continuously adds the latest data, which is conducive to improving the estimation accuracy.

- (3) It is proposed to adopt the internal degradation feature (ohmic internal resistance increment) and external degradation feature (voltage sample entropy) as well as capacity degradation together as inputs to the LSTM degradation state model, which conveys diversified aging information and enhances the learning and estimation performance of the model.
- (4) Variational mode decomposition (VMD) is used to process the identified ohmic internal resistance to obtain the main trend of ohmic internal resistance with state of charge (SoC).

Following is the arrangement for the remaining portions of this essay: Section 2 provides the experiments' specifics. Section 3 introduces the extraction of degradation indicators, establishment of a degradation state model, and SoH estimate using MM-LSTM. In Section 4, the SoH estimation comparing findings and error analysis are presented. Finally, the conclusions and suggestions for further research are provided in Section 5.

## 2. Experiment

The experimental platform included a power supply (ITECH IT6523D from ITECH Electronics (ITECH) in Nanjing, China) and an electronic load (ITECH IT8816 from ITECH Electronics (ITECH) in Nanjing, China) for controlling battery charge–discharge, a temperature-controlled environment chamber, and a host computer that served as the main controller and data logger (Figure 1). The data sampling frequency was 1 Hz.

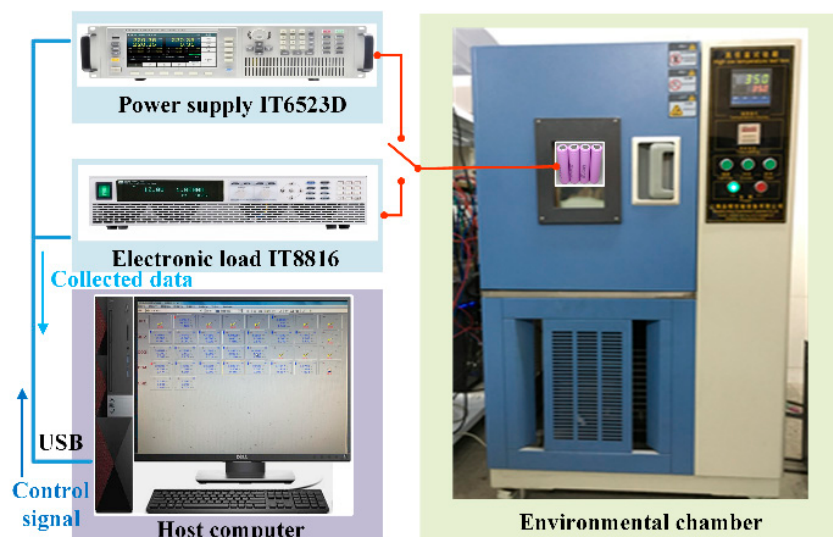


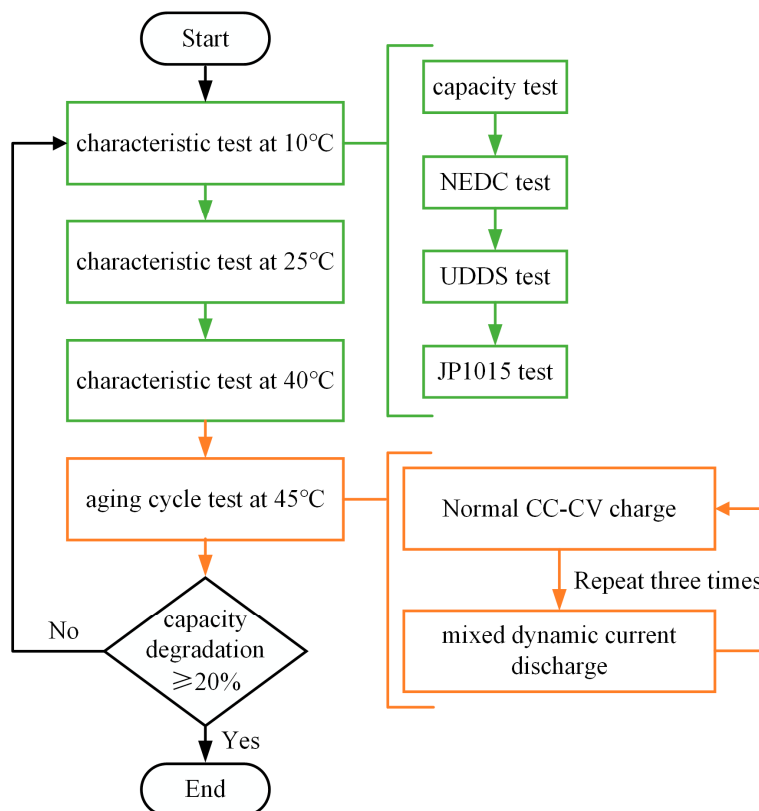
**Figure 1.** The battery test bench.

Two kinds of lithium-ion batteries were tested in this article: a LiNMC NCR18650B battery (labeled P01) from Panasonic (Osaka, Japan) and four LCO ICR18650-26F batteries (labeled S17, S30, S42, and S43) from Samsung (Seongnam, Gyeonggi-do, Republic of Korea). During the test, the batteries were placed in the environmental chamber and the battery test procedures (Table 1) were carried out individually.

For S42 and S43, the testing procedures in each test cycle included the characteristic tests at three temperatures ( $10^{\circ}\text{C}$ ,  $25^{\circ}\text{C}$ , and  $40^{\circ}\text{C}$ ) and the aging cycle tests (Figure 2). A capacity test and three dynamic condition tests were among the characteristic tests. The three dynamic operating condition tests were the New European Driving Cycle (NEDC), the Urban Dynamometer Driving Schedule (UDDS), and the Japanese 1015 Mode Driving Schedule (JP1015). The mixed dynamic current consisted of NEDC, UDDS, and JP1015.

**Table 1.** The contents of the battery test procedures.

Battery	Characteristic Tests		Aging Tests	
	Test Procedures	Temperature	Test Procedures	Temperature
S42/S43	Capacity test/ NEDC/UDDS/JP1015	10 °C/25 °C/40 °C	Mixed dynamic current	45 °C
S30	Capacity test/NEDC	35 °C	NEDC&2C-rate pulse	35 °C
S17	Capacity test/NEDC	25 °C	UDDS	45 °C
P01	Capacity test/UDDS	25 °C	UDDS	45 °C

**Figure 2.** Experimental test procedure for batteries S42 and S43.

For S30, S17, and P01, the test procedures also included characteristic tests and aging cycle tests. The characterization and aging tests formed a test cycle. The characteristic tests consisted of a capacity test and a single dynamic profile test, and the aging test procedures were repeated 10 times in each test cycle. More details about the test procedures of S30, S17, and P01 and discharge curves for dynamic profile tests (NEDC, UDDS, and JP1015) are presented in Ref. [32].

### 3. Methodology

The offline training phase and the online SoH estimation phase comprise the primary divisions of the developed battery SoH estimation framework based on the MM-LSTM algorithm (Figure 3). During the training phase, degradation indicators are extracted and reconstructed using the measured data from the battery testing. An LSTM model is then created using the degradation indicators as inputs. In the online SoH estimation phase, an LSTM-based degradation state model is rebuilt utilizing the parameters from the constructed LSTM training model. The degradation indicators that are taken from the online test data are used as the model's input. The inputs are updated through the metabolic process, and the estimated capacity degradation is obtained to further compute

SoH. Three parts make up the specific implementation: the extraction and reconstruction of degradation indicators, construction of LSTM-based battery degradation state model, and SoH estimate using MM-LSTM.

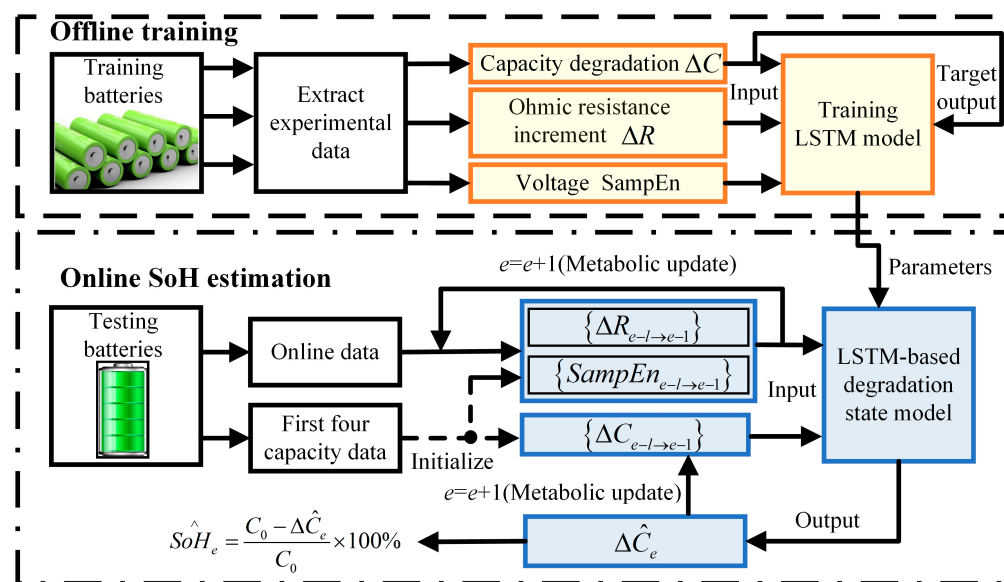


**Figure 3.** The MM-LSTM framework for SoH estimate.

### 3.1. Degradation Indicators Extraction and Reconstruction

The selection and extraction of appropriate degradation indicators are of significance for estimating battery SoH accurately and reliably [33]. The sample entropy (SampEn) can capture the subtle and complicated signal changes reliably during the battery aging process [34], and SampEn shows considerable sensitivity to capacity loss [35]. The increment of ohmic internal resistance ( $\Delta R$ ) is closely related to battery deterioration [36], and our earlier research [30] has pointed out the strong correlation between  $\Delta R$  and capacity loss. As a result, SampEn and  $\Delta R$  are selected as degradation indicators based on their established correlation with battery capacity loss.

#### 3.1.1. Sample Entropy Extraction

With the aging of the battery, the voltage response varies accordingly for the same discharge phase [37]. As an improved algorithm of approximate entropy, sample entropy itself does not depend on data length, and can effectively reflect the complexity of time series [38]. The SampEn is used to capture the fluctuation and complexity of the battery's voltage response as it ages. The voltage SampEn reflects the aging law of the battery based on the external parameters of the battery. The traditional calculation method of the SampEn needs to calculate all the vectors' similarity probability, which takes up a lot of computational resources and adds to the workload of BMS. To overcome this issue, a fast SampEn calculation method [39] is adopted in this research. The specific calculation procedure of the fast calculation method is detailed in Algorithm 1.

#### 3.1.2. Increment Extraction of Ohmic Internal Resistance

SoH estimation is usually based on the acquired battery health parameters, which can be obtained by modeling the battery. The use of experimental methods to obtain health parameters is not suitable for online estimation because of the long testing time and high equipment requirements. The Thevenin model is the greatest option for simulating battery dynamics due to its simplicity and efficiency, especially when taking into account the accuracy and complexity of equivalent circuit models [40]. Based on the Thevenin model,

real-time monitoring data can be used to identify the internal resistance for the online estimation of SoH. The Thevenin model consists of a Resistance–Capacitance (RC) network, a series resistor ( $R_0$ ), and an ideal voltage source (Figure 4).

---

**Algorithm 1** The calculation process of the sample entropy.

---

Step 1: Form a time series matrix. For a time series of length  $n$ ,

$\{v(n)\} = v(1), v(2), \dots, v(n)$ , assign the dimension  $m$  and similarity threshold  $r$ . The

$$\text{time series matrix } D \text{ is defined as } D = \begin{bmatrix} v(1) & v(2) & \cdots & v(1+m) \\ \vdots & \vdots & & \vdots \\ v(i) & v(i+1) & \cdots & v(i+m) \\ \vdots & \vdots & & \vdots \\ v(n-m) & v(n-m+1) & \cdots & v(n) \end{bmatrix}.$$

Step 2: Calculate the distance matrix. The equation of each element is as follows:

$$d_i(k-i, j) = |D(k, j) - D(i, j)|, (i+1 \leq k \leq n-m, 1 \leq j \leq m+1)$$

The distance matrix  $d$  can be summarized as

$$d = \begin{bmatrix} |v(i+1) - v(i)| & |v(i+2) - v(i+1)| & \cdots & |v(i+1+m) - v(i+m)| \\ \vdots & \vdots & & \vdots \\ |v(n-m) - v(i)| & |v(n-m+1) - v(i)| & \cdots & |v(n) - v(i)| \end{bmatrix}_{(n-m-i) \times (m+1)}$$

Step 3: Obtain the number of template matching in  $m$ -dimension and  $m+1$ -dimension.

$$B_i^m = \text{the number of } \left[ \max_{1 \leq j \leq m} (d_i(p, j)) < r \right], (1 \leq p \leq n-m-i)$$

$$B_i^{m+1} = \text{the number of } \left[ \max_{1 \leq j \leq m+1} (d_i(p, j)) < r \right], (1 \leq p \leq n-m+1-i)$$

Step 4: Sum the number of matching templates in  $m$ -dimension and  $m+1$ -dimension.

$$B_m = \sum_{i=1}^{n-m} B_i^m, B_{m+1} = \sum_{i=1}^{n-m} B_i^{m+1}.$$

Step 5: The sample entropy is calculated.

$$\text{SampEn}(m, r, n) = -\ln \left[ \frac{B^{m+1}}{B^m} \right]$$


---

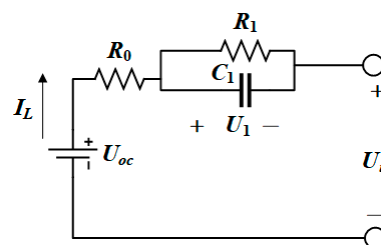


**Figure 4.** The Thevenin model. Adapted from [4].

The analytical equation of the Thevenin model is written as follows:

$$\begin{cases} U_{oc} = U_t + I_L R_0 + U_1 \\ I_L = \frac{U_1}{R_1} + C_1 \frac{dU_1}{dt} \end{cases} \quad (1)$$

where  $U_{oc}$  represents the OCV of the battery,  $U_t$  denotes the terminal voltage,  $I_L$  denotes the load current,  $R_1$  and  $C_1$  stand for the polarization resistance and polarization capacitance, respectively,  $R_0$  is the ohmic resistance, and  $U_1$  is the polarization voltage.

During operation, the charge/discharge voltage and load current of lithium-ion batteries are readily detected and measured. After modeling, the battery parameter  $R_0$  was identified in real-time under dynamic loading profiles using the recursive least square

with a forgetting factor (FFRLS) algorithm [41–43]. The forgetting factor was set as 0.95. A small forgetting factor is beneficial for enhancing system tracking capability, but it could cause bigger fluctuations [44]. And, ohmic internal resistance identification is mostly influenced by noise without regularity, and the ohmic internal resistance derived from direct parameter identification is insufficiently stable under complex loading profiles [45]. The presence of fluctuations is not conducive to the proper calculation of degradation indicators. In this case, variational mode decomposition (VMD) [46] is adopted to decompose the ohm internal resistance signal, and the major trend of the signal is extracted by removing the high-frequency signal and retaining the low-frequency signal. The key of VMD is to decompose the original signal into several intrinsic mode functions (IMFs) for minimizing the sum of the estimated bandwidth of each IMF. Specific steps of VMD are summarized in Algorithm 2. The decomposition result of the ohmic internal resistance signal is shown in Figure 5.

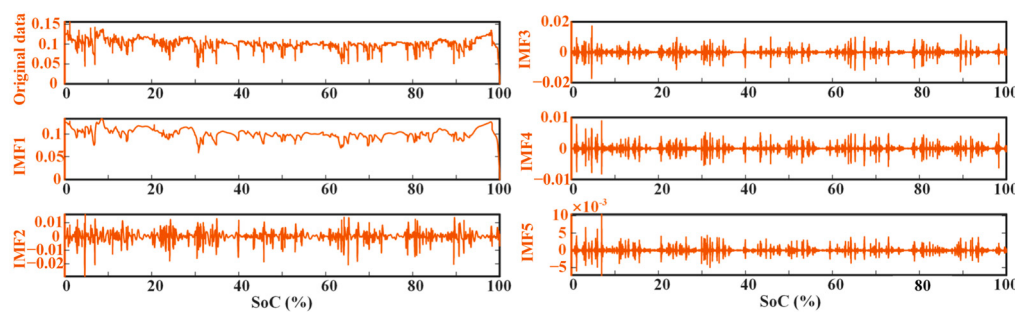


**Figure 5.** Ohmic internal resistance decomposition result by VMD.

According to previous research [41], the batteries in EVs typically function under the conditions of 25–95% SoC in practice, and the trend of identified ohmic internal resistance is essentially constant when the SoC is between 30% and 80%. In light of this, the average of ohmic internal resistance for 30–80% SoC is considered a sign of particular aging stages. The expression of the average ohmic internal resistance  $R_e^{ave}$  is as follows:

$$R_e^{ave} = \frac{1}{n}(R_e^{SoC=30\%} + \dots + R_e^{SoC=80\%}) \quad (2)$$

where  $n$  is the sequence's number of elements and  $R_e^{SoC}$  is the ohmic internal resistance of the  $e$ -th cycle at certain SoC. The SoC is determined by utilizing the Coulomb-counting method.

However, the initial ohmic internal resistance of different batteries is diverse, even if the batteries are produced in the same batch. Meanwhile, the ohmic internal resistance is significantly influenced by ambient temperature. These realities hinder the direct application of the mean ohmic internal resistance. Therefore, the increase in ohmic internal resistance  $\Delta R$  is proposed as one of the degradation indicators. The corresponding expression is as follows:

$$\Delta R_e = R_e^{ave} - R_0^{ave} \quad (3)$$

where the  $R_0^{ave}$  is the initial average ohmic internal resistance and  $\Delta R_e$  is the increase in ohmic internal resistance of the  $e$ -th cycle.

---

**Algorithm 2** The calculation process of variational mode decomposition.
 

---

Step 1: Hilbert transform.

The original signal  $f(t)$  can be divided into  $K$  IMFs. Each IMF  $u_k(t)$  is performed through Hilbert transformation and modulates the frequency spectrum to the corresponding baseband by incorporating an exponential component to enhance the model's adaptability  $e^{-j\omega_k t} \left[ \left( \delta(t) + \frac{j}{\pi t} \right) * u_k(t) \right] e^{-j\omega_k t}$ .

where  $\delta(t)$  is the Dirac function,  $j^2 = -1$ , and  $\omega_k$  denotes the center frequency.

Step 2: Constructing constrained variational problem.

The bandwidth of the demodulated signal is calculated by Gaussian smoothness, and the objective function can be expressed as follows:

$$\begin{cases} \min_{\{u_k\}, \{\omega_k\}} \left\{ \sum_{k=1}^K \left\| \partial_t \left[ \left( \delta(t) + \frac{j}{\pi t} \right) * u_k(t) \right] e^{-j\omega_k t} \right\|_2^2 \right\} \\ \text{s.t.} \quad \sum_{k=1}^K u_k(t) = f(t) \end{cases}$$

Step 3: Unconstrained variational problem transformation [47].

Lagrange multiplier operator  $\lambda(t)$  and penalty factor  $\alpha$  are introduced to convert the constrained variational problem into an unconstrained variational problem:

$$L(\{u_k\}, \{\omega_k\}, \lambda) = \alpha \sum_{k=1}^K \left\| \partial_t \left[ \left( \delta(t) + \frac{j}{\pi t} \right) * u_k(t) \right] e^{-j\omega_k t} \right\|_2^2 + \left\| f(t) - \sum_{k=1}^K u_k(t) \right\|_2^2 + \left\langle \lambda(t), f(t) - \sum_{k=1}^K u_k(t) \right\rangle$$

Step 4: Updating IMF and center frequency.

Initialize the  $\{\hat{u}_k^1\}$ ,  $\{\omega_k^1\}$ ,  $\hat{\lambda}^1$ , and  $n$ , and then update IMF, center frequency, and Lagrange multiplier until the cut-off condition is reached. The update process can be denoted as follows:

$$\hat{u}_k^{n+1}(\omega) = \frac{\hat{f}(\omega) - \sum_{i=1, i \neq k}^K \hat{u}_i(\omega) + \frac{\hat{\lambda}(\omega)}{2}}{1 + 2\alpha(\omega - \omega_k)^2}, \quad \omega_k^{n+1} = \frac{\int_0^\infty \omega |\hat{u}_k(\omega)|^2 d\omega}{\int_0^\infty |\hat{u}_k(\omega)|^2 d\omega},$$

$$\hat{\lambda}^{n+1}(\omega) = \hat{\lambda}^n(\omega) + \gamma \left[ \hat{f}(\omega) - \sum_{k=1}^K \hat{u}_k^{n+1}(\omega) \right].$$

$$\text{The update cut-off condition is as follows: } \sum_{k=1}^K \frac{\|\hat{u}_k^{n+1} - \hat{u}_k^n\|_2^2}{\|\hat{u}_k^n\|_2^2} < \varepsilon$$

where  $n$  denotes the number of iterations and  $\varepsilon$  is discriminant accuracy.

---

### 3.2. Establishment of Degradation State Model Based on LSTM

Battery deterioration is a non-linear time-varying process, and each cycle's aging parameters have a strong relationship with those of the cycle before it [22]. To represent the intricate deterioration mechanisms that are challenging to quantify by fitting a particular mathematical equation, a battery degradation state model is developed using the capacity degradation as the estimated state variable and the extracted degradation indicators as input observation variables. The extracted degradation indicators are added as the observation compensations to reflect the change in aging characteristics and modify the model. These variables' correlation can be roughly represented as follows:

$$\Delta C_e = f(\Delta C_{e-1}, SampEn_{e-1}, \Delta R_{e-1}) \quad (4)$$

where  $\Delta C_e$  is capacity degradation at the  $e$ -th cycle, and  $f(\Delta C_{e-1}, SampEn_{e-1}, \Delta R_{e-1})$  is the function describing degradation mechanisms.

However, it is nearly impossible to obtain an exact analytical formula for Equation (4) because of the intricate electrochemical reaction mechanism occurring inside the battery

during aging. To approximate Equation (4) in this situation, the LSTM algorithm is applied. LSTM is an improved version of RNN, and it can solve the problem of RNN's gradient vanishing and exploding during backward propagation [48,49]. Due to its simpler structure and effectiveness in interpreting variable-sized time-series battery data, LSTM is found to perform better than alternative model architectures for battery capacity estimation [50]. The context unit is intricately designed by the LSTM layers employing three gates. The fundamental components of the LSTM algorithm are the input gate, forget gate, and output gate (Figure 6), which are in charge of receiving signals, removing unnecessary information, and outputting estimation, respectively [51].

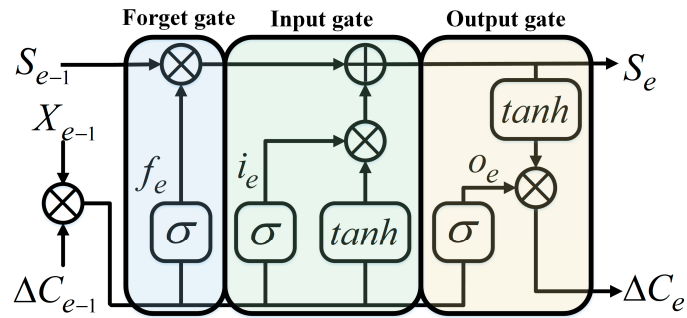


**Figure 6.** The schematic diagram of LSTM.

The sigmoid activation function and hyperbolic tangent function are used to obtain the cell state. Relevant expressions are summarized as Equation (5):

$$\left\{ \begin{array}{l} f_e = \sigma(W_{f1}X_{e-1} + W_{f2}\Delta C_{e-1} + b_f) \\ i_e = \sigma(W_{i1}X_{e-1} + W_{i2}\Delta C_{e-1} + b_i) \\ o_e = \sigma(W_{o1}X_{e-1} + W_{o2}\Delta C_{e-1} + b_o) \\ S_e = f_e \odot S_{e-1} + i_e \odot \tanh(W_{s1}X_{e-1} + W_{s2}\Delta C_{e-1} + b_c) \\ \Delta C_e = o_e \odot \tanh(S_e) \end{array} \right. \quad (5)$$

where  $f$ ,  $i$ ,  $o$ , and  $S$  denote forget gate, input gate, output gate, and cell state, respectively;  $b$  denotes bias parameter;  $W$  is network weight;  $\odot$  denotes the point-wise multiplication;  $\sigma$  is the sigmoid function;  $\tanh$  is the hyperbolic tangent function; and  $X = [\Delta C, SampEn, \Delta R]$  is degradation indicator.

### 3.3. MM-LSTM for Battery SoH Estimation

Multiple indicators are required to convey information about battery aging since the change in battery SoH is a typically non-linear and slow time-varying process, and the latest data are needed to accurately reflect the trend in battery deterioration. Accordingly, the multiple inputs and metabolic mechanisms are merged into the LSTM-based degradation state model to produce a precise SoH estimate of battery in the situation of a limited number of data samples. Degradation indicators that have been extracted and capacity loss are inputs to the LSTM-based degradation state model, and the metabolic process is employed to update the model's inputs. After the estimating process has begun, the succeeding battery capacity information is unknown in the online application. In the circumstances, the estimated capacity data ought to be used as a true value for the iteration process. The detailed estimation procedures are expressed as follows:

Step 1: Initial estimate of capacity degradation.

Collecting the historical data of the battery's first  $l$  cycles, the capacity degradation is calculated directly from the recorded capacity data, and the degradation indicators are extracted using the method in Section 3.1 under dynamic operating conditions. The

resulting capacity degradation and degradation indicators together form the historical sequences. The historical sequences from the  $(e-l)$ -th to  $(e-1)$ -th ( $l$  is set as 4) cycle are written as Equation (6):

$$\begin{cases} \{\Delta C_{e-l \rightarrow e-1}\} = \{\Delta C_{e-l}, \Delta C_{e-l+1}, \dots, \Delta C_{e-1}\} \\ \{SampEn_{e-l \rightarrow e-1}\} = \{SampEn_{e-l}, SampEn_{e-l+1}, \dots, SampEn_{e-1}\} \\ \{\Delta R_{e-l \rightarrow e-1}\} = \{\Delta R_{e-l}, \Delta R_{e-l+1}, \dots, \Delta R_{e-1}\} \end{cases} \quad (6)$$

To complete the initial estimation of capacity degradation, the sequences in Equation (6) constitute the input of the developed LSTM-based degradation state model  $f_{LSTM}(\bullet)$ , and the capacity degradation of the adjacent cycle is estimated. The process of estimation is expressed as Equation (7):

$$\Delta \hat{C}_e = f_{LSTM}(\{\Delta C_{e-l \rightarrow e-1}\}, \{SampEn_{e-l \rightarrow e-1}\}, \{\Delta R_{e-l \rightarrow e-1}\}) \quad (7)$$

where the  $\Delta \hat{C}_e$  is the estimated capacity degradation of the  $e$ -th aging cycle.

Step 2: SoH estimation.

The battery SoH of the  $e$ -th aging cycle can be determined using Equation (8) in accordance with the definition of SoH:

$$\hat{SoH}_e = \frac{C_0 - \Delta \hat{C}_e}{C_0} \times 100\% \quad (8)$$

where the  $C_0$  denotes the rated capacity of a new battery.

Step 3: The metabolic updating

The major purpose of employing the metabolic mechanisms is to use the latest data available for estimation. Thus, the inputs of the model  $f_{LSTM}(\bullet)$  will be updated once a new capacity degradation is obtained by estimation. As an example, after the capacity degradation of the  $e$ -th cycle ( $\Delta \hat{C}_e$ ) has been estimated, the capacity deterioration data of the  $(e-l)$ -th cycle ( $\Delta C_{e-l}$ ) will be removed and the latest estimated capacity degradation ( $\Delta \hat{C}_e$ ) will be introduced to construct a new capacity degradation sequence. Meanwhile, degradation indicators for the present aging cycle ( $SampEn_e$  and  $\Delta R_e$ ) are online extracted by gathering data in real-time while the battery is being used. The degradation indicator sequences are updated by removing the degradation indicator data from the  $(e-l)$ -th cycle and adding the degradation indicator data from the  $e$ -th cycle. These updated sequences will be used to produce the new input data sequences of the LSTM-based degradation state model. The new input data sequences are expressed as Equation (9).

$$\begin{cases} \{\Delta C_{e-l+1 \rightarrow e}\} = \{\Delta C_{e-l+1}, \Delta C_{e-l+2}, \dots, \Delta \hat{C}_e\} \\ \{SampEn_{e-l+1 \rightarrow e}\} = \{SampEn_{e-l+1}, SampEn_{e-l+2}, \dots, SampEn_e\} \\ \{\Delta R_{e-l+1 \rightarrow e}\} = \{\Delta R_{e-l+1}, \Delta R_{e-l+2}, \dots, \Delta R_e\} \end{cases} \quad (9)$$

The LSTM-based degradation state model  $f_{LSTM}(\bullet)$  receives the new input data sequences formed by Equation (9) and estimates the capacity degradation. Go back to Step 2 and estimate the SoH for the following cycle. The SoH over the battery's whole life cycle is precisely estimated by repeating Steps 2 and 3 until the anticipated capacity loss approaches the cut-off criterion (20% of the rated capacity).

## 4. Results and Discussion

### 4.1. SoH Estimation for Different Inputs with Metabolic LSTM

The SoH estimation for different inputs was carried out to validate the advantages of the proposed multiple inputs model. As a benchmark comparison, various inputs such as

$\Delta C$ ,  $\Delta R$ ,  $SampEn$ ,  $\Delta C + \Delta R$ ,  $\Delta C + SampEn$ , and  $\Delta R + SampEn$  were employed to evaluate the efficacy of multiple inputs  $\Delta C + \Delta R + SampEn$  ( $CREn$ ). The LSTM-based degradation state model was trained offline using the data from S43\_25 °C\_NEDC during offline training, while the data from S42\_25 °C\_UDDS were used for the initialization of estimation and SoH prediction following steps 1 to 3 in Section 3.3. The SoH estimation results for various inputs are summarized in Table 2.

**Table 2.** Errors in the battery SoH estimation for various inputs.

Input	$\Delta C$	$\Delta R$	$SampEn$	$\Delta C + \Delta R$	$\Delta C + SampEn$	$\Delta R + SampEn$	$CREn$
Max AE	2.32	4.67	3.37	2.25	2.24	2.31	1.49
MAE	0.81	1.01	1.26	0.72	0.79	1.19	0.38
RMSE	0.90	1.44	1.46	0.83	0.89	1.39	0.49

The evaluation metrics for battery SoH estimation performance include the maximum absolute error (Max AE), mean absolute error (MAE), and root mean square error (RMSE). Among all the inputs, Max AE was significantly the largest when using  $\Delta R$  alone as the input, exceeding twice the Max AE of the proposed multiple inputs ( $CREn$ ). When  $SampEn$  was used as the input, the Max AE reached 3.37%, which was also relatively high. The Max AE of the two-indicator input models was consistently lower than that of the single-indicator input models, while the three-indicator combination input ( $CREn$ ) achieved the smallest Max AE. Furthermore, Max AE, MAE, and RMSE all reached minimum values for the proposed multiple inputs ( $CREn$ ), demonstrating superior estimation accuracy compared to other input configurations.

The degradation indicators of lithium-ion batteries in real-world operational conditions include local regenerations, noise fluctuations, and overall battery deterioration trends. Their inherent non-linear and non-smooth characteristics contribute to suboptimal estimating performance when relying on a single input [52]. By incorporating multiple indicators, the proposed approach effectively accounted for various factors affecting battery aging, thereby enhancing the tracking of battery aging.

In conclusion, employing the suggested indicators ( $CREn$ ) as the inputs of the metabolic LSTM allowed the SoH estimate framework to achieve optimal estimation performance.

#### 4.2. SoH Estimation for the Same Type of Batteries with MM-LSTM

To verify the accuracy of the estimation and the generalizability of the suggested MM-LSTM framework, the SoH estimates for the same type of batteries under different operating scenarios were conducted. The LCO ICR18650-26F batteries were used for offline training and online estimation. Using S43\_25 °C\_UDDS as a reference battery for offline training, an LSTM-based degradation state model was established. To estimate battery SoH, data from batteries operating at various temperatures and loading profiles were employed. The outcomes of the SoH estimates are displayed in Figure 7. Test points indicate the number of test cycles. The battery test data and estimation errors are summarized in Table 3.

The true SoH trajectory of S17\_25 °C\_NEDC exhibits local oscillations during the early aging process but is comparatively smooth throughout the subsequent phase (Figure 7a). As a result, the beginning of degradation is when SoH estimation error is at its highest. The SoH estimation errors after that exhibit a trend of fluctuating convergence. Early on in aging, the SoH degradation trend of S30\_35 °C\_NEDC (Figure 7b) is quite mild. Capacity recovery happens at the middle stage of degradation as a result of the experimental period's adjustment, which causes comparable fluctuation in the SoH trajectory. This occurrence results in a maximum error in the estimation of SoH that corresponds to the fluctuation

point. Additionally, in the later stages of aging, the SoH trajectory exhibits a notable accelerated decline, which causes the SoH estimation error to increase somewhat, but eventually converges to 0. The SoH trajectory of S42\_40 °C\_JP1015 (Figure 7d) exhibits a similar fluctuation due to the battery's capacity recovering while the experiment is suspended. The estimated SoH in this instance continues to closely match the true SoH trajectory. The SoH trajectory of S42\_10 °C\_UDDS is comparatively smooth (Figure 7c). During the early phases of degradation, the estimated SoH values closely follow the real SoH trend. The projected SoH values during the intermediate stages of aging differ slightly from the actual SoH trajectory, but the estimation error is less than 1.1%. Moreover, as degradation progresses, the estimated SoH gradually converges to the true SoH.

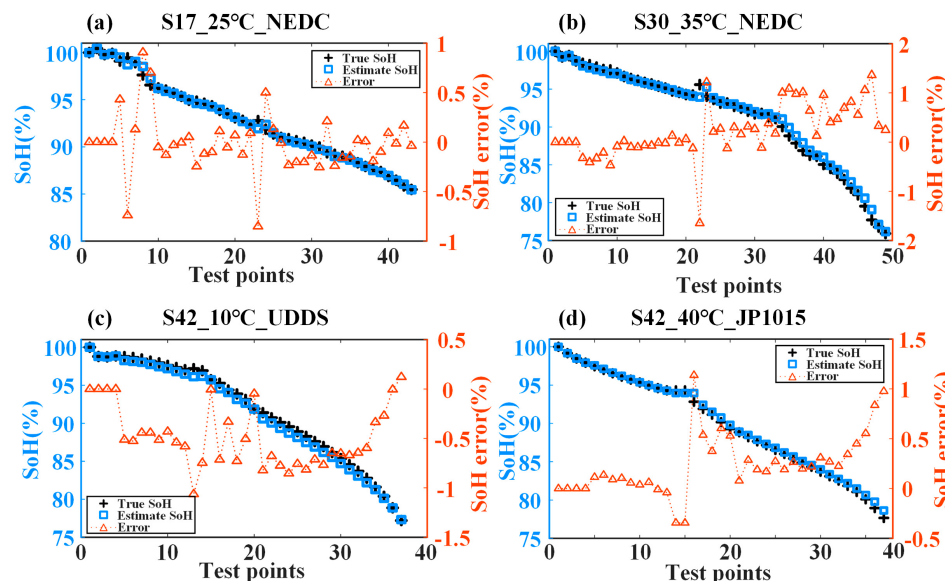


**Figure 7.** The SoH estimation outcomes for identical battery types under various operating conditions (S43\_25 °C\_UDDS for offline training).

**Table 3.** The SoH estimation errors for identical battery types under various operating conditions (S43\_25 °C\_UDDS for offline training).

Battery Test Data	Max AE (%)	MAE (%)	RMSE
S17_25 °C_NEDC	0.905906	0.184919	0.291184
S30_35 °C_NEDC	1.659912	0.416245	0.598103
S42_10 °C_UDDS	1.068272	0.511968	0.593807
S42_40 °C_JP1015	1.128570	0.267430	0.376193

It is also important to note that the test cells' SoH was evaluated at various temperatures or dynamic loading profiles. The maximum RMSE was 0.5981, while the Max AE and MAE of the estimated SoH were both less than 1.66% and 0.52%, respectively. This shows that the predicted SoH values are quite near to the actual SoH values. The aforementioned findings demonstrate that the proposed MM-LSTM framework has effective transfer application capabilities for the same type of batteries under various working situations.

#### 4.3. SoH Estimation for the Different Types of Batteries with MM-LSTM

In order to further confirm the estimation effectiveness and generalizability of the suggested MM-LSTM framework, test data from cells with different cathode materials were used to estimate SoH. For offline training, the P01 (LiNMC cathode) as a reference battery was used to build the LSTM-based degradation state model. As test batteries, S17, S30, S43, and S42 (LCO cathode) were used for estimation initialization, and the SoH for their entire

life cycle was estimated. The SoH estimation outcomes under various working situations are displayed in Figure 8. The battery test data and estimation errors are summarized in Table 4.

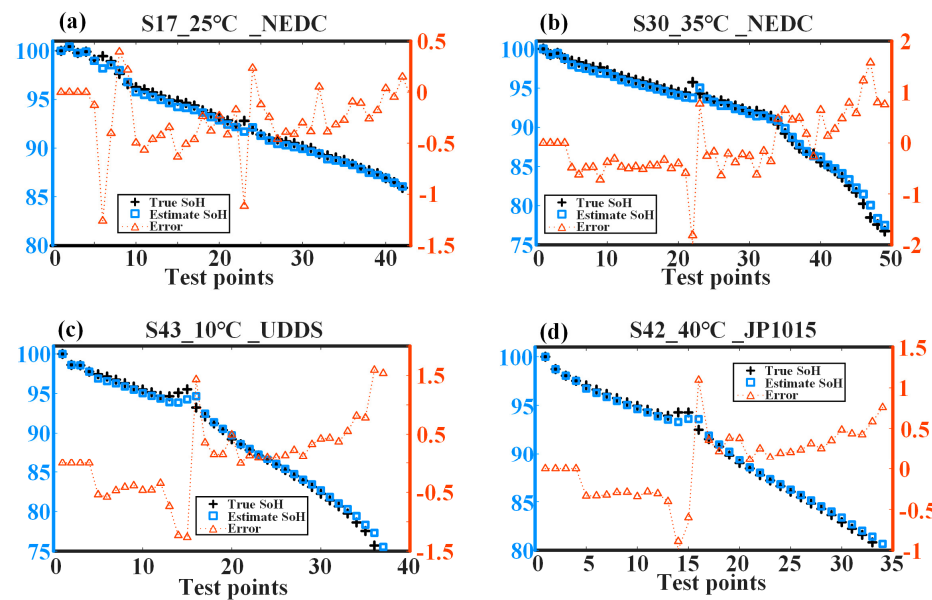


**Figure 8.** The SoH estimation outcomes for different battery types under various operating conditions (P01\_25 °C\_UDDS for offline training).

**Table 4.** The SoH estimation errors for different battery types under various operating conditions (P01\_25 °C\_UDDS for offline training).

Battery Test Data	Max AE (%)	MAE (%)	RMSE
S17_25 °C_NEDC	1.208814	0.278034	0.369471
S30_35 °C_NEDC	1.979489	0.484944	0.606126
S43_10 °C_UDDS	1.596516	0.468006	0.637837
S42_40 °C_JP1015	1.115515	0.345183	0.422632

Similarly to Figure 7, these LCO cells' true SoH trajectories exhibit significant fluctuations (Figure 8a–d); however, despite deviations at various phases of degradation, the SoH estimated by the model trained by P01 still displays a good level of agreement with the actual SoH. The four test batteries are tested at different working conditions. But, the four batteries' SoH estimation errors are less than 2%, demonstrating that the LSTM-based deterioration state model trained by P01 can accurately estimate SoH for other battery types with diverse cathode materials, even while operating under various working situations. For different battery types, the MAE of SoH estimate is no more than 0.49%, and the highest RMSE is 0.6378. The created LSTM-based degradation state model's ability to accurately depict the typical deterioration mechanism of batteries with diverse cathode materials is the cause of the estimation's high accuracy. Additionally, the metabolic mechanism in conjunction with the multi-input components precisely tracks the battery's aging trend and reflects variations in the internal properties of the battery. The SoH estimate results firmly confirm that the LSTM framework combined with multiple inputs and metabolism has superior transfer application capabilities for different battery kinds.

#### 4.4. SoH Estimation for Different Algorithms

To highlight the superiority of the MM-LSTM, the LSTM, GPR, and SVM were each employed as comparison algorithms for SoH estimation under different scenarios. Degrade-

dation indicators were used directly as input and the related capacity degradation as the output throughout the training procedure of the comparison algorithm. The proposed degradation indicators were employed as inputs to estimate SoH. The estimation outcomes are displayed in Figure 9, and Table 5 provides a summary of the estimation errors.

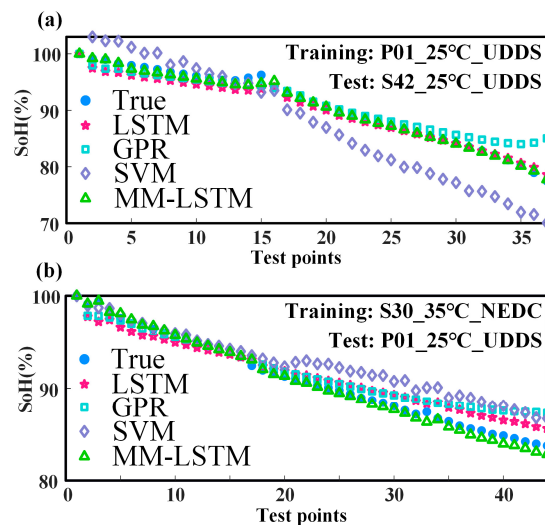


**Figure 9.** The SoH estimation outcomes for different algorithms. (a) The SoH estimation results of different algorithms for S42\_25 °C\_UDDS (Tranning: P01\_25 °C\_UDDS). (b) The SoH estimation results of different algorithms for P01\_25 °C\_UDDS (Tranning: S30\_35 °C\_NEDC).

**Table 5.** Errors in SoH estimate for various algorithms.

Estimation Conditions			Max AE (%)	MAE (%)	RMSE
Training	Test	Method			
P01_25 °C_UDDS	S42_25 °C_UDDS	MM-LSTM	1.472084	0.339361	0.493987
		LSTM	2.547781	1.377743	1.509782
		GPR	7.565608	1.384660	2.004434
		SVM	8.576399	4.385365	5.055987
S30_35 °C_NEDC	P01_25 °C_UDDS	MM-LSTM	1.102647	0.367896	0.471806
		LSTM	2.254128	1.003433	1.143148
		GPR	3.600902	1.187140	1.597829
		SVM	3.394373	1.837639	2.185471

Clearly, the estimated SoH trajectories using GPR and SVM diverge from the actual SoH trajectory to varied degrees (Figure 9a,b). This phenomenon happens as a result of the differing training and test cells, which causes a big discrepancy between the estimated and actual degradation trajectories. However, in this case, the estimation results of LSTM and MM-LSTM still show good accuracy. The LSTM algorithm is more accurate than the GPR and SVM algorithms at estimating SoH. This is due to the fact that the gated recurrent unit of the LSTM is employed to regulate the gradient information's propagation, which in turn controls the degree of memory and forgetting of prior and present information. But, the SoH estimation accuracy of LSTM is not as good as that of MM-LSTM. In these cases, the SoH estimated by MM-LSTM has the smallest Max AE, MAE, and RMSE among the four algorithms (Table 5). These findings show that the MM-LSTM for estimating SoH has the best estimation accuracy and stability and exhibits good generalization ability. The MM-LSTM always estimates SoH using degradation indicators drawn from the most recent battery data due to the introduction of the metabolism, which can faithfully reflect the deterioration trend of the battery. In conclusion, these findings further demonstrate the

exceptional performance and generalizability of the suggested MM-LSTM framework for the SoH estimation of different battery types.

## 5. Conclusions

In this research, the performance and applicability of the MM-LSTM system for SoH estimation were evaluated with the help of data from two distinct types of batteries operating under various situations. The  $\Delta R$  produced by the FFRLS technique and VMD analysis and the *SampEn* extracted from discharge voltage were used as degradation indicators. Adopting different indicators ( $\Delta C$ ,  $\Delta R$ , *SampEn*,  $\Delta C + \Delta R$ ,  $\Delta C + \text{SampEn}$ ,  $\Delta R + \text{SampEn}$ , and *CREn*) as the input of metabolic LSTM framework, the estimation results showed that the framework obtained optimal estimation accuracy when the *CREn* were used as input. An LSTM-based degradation state model was used to specify the intricate degradation mechanism between adjacent cycles in this MM-LSTM framework. Additionally, the accuracy and generalizability of SoH estimation were enhanced by the incorporation of metabolic mechanisms and multiple inputs into the LSTM model.

The Max AE of SoH estimate for the same type of batteries under various temperatures or loading profiles was less than 1.7% and RMSE was within 0.6%, indicating that the MM-LSTM framework exhibited strong estimation performance under various test conditions. Meanwhile, the Max AE of SoH estimate for different kinds of cells was within 1.98%, and the RMSE did not exceed 0.64%, demonstrating the outstanding performance of the MM-LSTM framework for the transfer application between cells with distinct cathode materials (LCO and LiNMC) under various operating conditions. Additionally, the RMSE of SoH estimated by the MM-LSTM algorithm was 0.49%, which is the smallest among the four algorithms. The MM-LSTM approach obtained higher SoH estimate accuracy with a small amount of data than the other three data-driven algorithms (LSTM, GPR, and SVM). The findings of this study demonstrated that the metabolic LSTM framework combined with multiple inputs had remarkable transfer application capability, high accuracy, and generality in SoH estimation.

To enable the use of this estimating framework in battery management systems (BMSs) and expand the range of BMS applications in SoH, the proposed MM-LSTM framework will be integrated into the hardware platform in future research. Additionally, the current research has demonstrated that the degradation model can produce estimation with a higher degree of accuracy when given multiple indicators as input. Consequently, in future studies, other degradation indicators can be added to better track battery aging, such as fuzzy entropy, differential voltage analysis, polarization internal resistance, etc. Meanwhile, the LSTM algorithm can be integrated with other deep learning algorithms to improve the feature extraction ability of input data. Further implementation of the transfer application for SoH estimation between Li-ion ternary batteries and Li-FePO<sub>4</sub> batteries will continue to improve the accuracy of the LSTM transfer application for estimating battery SoH.

**Author Contributions:** L.C.: conceptualization, funding acquisition, writing—original draft, supervision, and project administration. D.C.: methodology, software, writing—review and editing, and formal analysis. M.H.: investigation and visualization. H.P.: resources, supervision, and project administration. B.J.: methodology and formal analysis. All authors have read and agreed to the published version of the manuscript.

**Funding:** This research was funded by the National Natural Science Foundation of China (Grant No. 52067003), Guangxi Key Lab of Manufacturing System and Advanced Manufacturing Technology (Grant No. 22-035-4S013).

**Data Availability Statement:** Data are contained within the article.

**Conflicts of Interest:** The authors declare no conflicts of interest.

## References

1. Feng, F.; Hu, X.; Liu, K.; Che, Y.; Linc, X.; Jin, G.; Liu, B. A Practical and Comprehensive Evaluation Method for Series-Connected Battery Pack Models. *IEEE Trans. Transp. Electrif.* **2020**, *6*, 391–416. [[CrossRef](#)]
2. Redondo-Iglesias, E.; Venet, P.; Pelissier, S. Modelling Lithium-Ion Battery Ageing in Electric Vehicle Applications—Calendar and Cycling Ageing Combination Effects. *Batteries* **2020**, *6*, 14. [[CrossRef](#)]
3. Shen, D.; Wu, L.; Kang, G.; Guan, Y.; Peng, Z. A novel online method for predicting the remaining useful life of lithium-ion batteries considering random variable discharge current. *Energy* **2021**, *218*, 119490. [[CrossRef](#)]
4. Chen, L.; Ding, Y.; Wang, H.; Wang, Y.; Liu, B.; Wu, S.; Li, H.; Pan, H. Online Estimating State of Health of Lithium-Ion Batteries Using Hierarchical Extreme Learning Machine. *IEEE Trans. Transp. Electrif.* **2022**, *8*, 965–975. [[CrossRef](#)]
5. Xiong, R.; Li, L.; Tian, J. Towards a smarter battery management system: A critical review on battery state of health monitoring methods. *J. Power Sources* **2018**, *405*, 18–29. [[CrossRef](#)]
6. Pradhan, S.K.; Chakraborty, B. Battery management strategies: An essential review for battery state of health monitoring techniques. *J. Energy Storage* **2022**, *51*, 104427. [[CrossRef](#)]
7. Ren, P.; Wang, S.; Chen, X.; Huang, J.; He, M. Fusion estimation strategy based on dual adaptive Kalman filtering algorithm for the state of charge and state of health of hybrid electric vehicle Li-ion batteries. *Int. J. Energy Res.* **2022**, *46*, 7374–7388. [[CrossRef](#)]
8. Li, X.; Yuan, C.; Wang, Z.; He, J.; Yu, S. Lithium battery state-of-health estimation and remaining useful lifetime prediction based on non-parametric aging model and particle filter algorithm. *Etransportation* **2022**, *11*, 100156. [[CrossRef](#)]
9. Pan, H.; Chen, C.; Gu, M. A State of Health Estimation Method for Lithium-Ion Batteries Based on Improved Particle Filter Considering Capacity Regeneration. *Energies* **2021**, *14*, 5000. [[CrossRef](#)]
10. Wu, T.; Liu, S.; Wang, Z.; Huang, Y. SOC and SOH Joint Estimation of Lithium-Ion Battery Based on Improved Particle Filter Algorithm. *J. Electr. Eng. Technol.* **2022**, *17*, 307–317. [[CrossRef](#)]
11. Zhu, F.; Fu, J.-Q. A Novel State-of-Health Estimation for Lithium-Ion Battery via Unscented Kalman Filter and Improved Unscented Particle Filter. *IEEE Sens. J.* **2021**, *21*, 25449–25456. [[CrossRef](#)]
12. Jiang, S.; Song, Z. A review on the state of health estimation methods of lead-acid batteries. *J. Power Sources* **2022**, *517*, 230710. [[CrossRef](#)]
13. Mc Carthy, K.; Gullapalli, H.; Ryan, K.M.; Kennedy, T. Review—Use of Impedance Spectroscopy for the Estimation of Li-ion Battery State of Charge, State of Health and Internal Temperature. *J. Electrochem. Soc.* **2021**, *168*, 080517. [[CrossRef](#)]
14. Stroe, D.-I.; Schaltz, E. Lithium-Ion Battery State-of-Health Estimation Using the Incremental Capacity Analysis Technique. *IEEE Trans. Ind. Appl.* **2020**, *56*, 678–685. [[CrossRef](#)]
15. Liu, G.; Ouyang, M.; Lu, L.; Li, J.; Han, X. Online estimation of lithium-ion battery remaining discharge capacity through differential voltage analysis. *J. Power Sources* **2015**, *274*, 971–989. [[CrossRef](#)]
16. Oji, T.; Zhou, Y.; Ci, S.; Kang, F.; Chen, X.; Liu, X. Data-Driven Methods for Battery SOH Estimation: Survey and a Critical Analysis. *IEEE Access* **2021**, *9*, 126903–126916. [[CrossRef](#)]
17. Feng, X.; Weng, C.; He, X.; Han, X.; Lu, L.; Ren, D.; Ouyang, M. Online State-of-Health Estimation for Li-Ion Battery Using Partial Charging Segment Based on Support Vector Machine. *IEEE Trans. Veh. Technol.* **2019**, *68*, 8583–8592. [[CrossRef](#)]
18. Yang, Y.; Wen, J.; Shi, Y.; Zeng, J. State of Health Prediction of Lithium-Ion Batteries Based on the Discharge Voltage and Temperature. *Electronics* **2021**, *10*, 1497. [[CrossRef](#)]
19. Song, L.; Zhang, K.; Liang, T.; Han, X.; Zhang, Y. Intelligent state of health estimation for lithium-ion battery pack based on big data analysis. *J. Energy Storage* **2020**, *32*, 101836. [[CrossRef](#)]
20. Wei, J.; Dong, G.; Chen, Z. Remaining Useful Life Prediction and State of Health Diagnosis for Lithium-Ion Batteries Using Particle Filter and Support Vector Regression. *IEEE Trans. Ind. Electron.* **2018**, *65*, 5634–5643. [[CrossRef](#)]
21. Li, Y.; Liu, K.; Foley, A.M.; Zülke, A.; Berecibar, M.; Nanini-Maury, E.; Van Mierlo, J.; Hoster, H.E. Data-driven health estimation and lifetime prediction of lithium-ion batteries: A review. *Renew. Sustain. Energy Rev.* **2019**, *113*, 109254. [[CrossRef](#)]
22. Chen, L.; Wang, H.; Liu, B.; Wang, Y.; Ding, Y.; Pan, H. Battery state-of-health estimation based on a metabolic extreme learning machine combining degradation state model and error compensation. *Energy* **2021**, *215*, 119078. [[CrossRef](#)]
23. Richardson, R.R.; Birk, C.R.; Osborne, M.A.; Howey, D.A. Gaussian Process Regression for In Situ Capacity Estimation of Lithium-Ion Batteries. *IEEE Trans. Ind. Inform.* **2019**, *15*, 127–138. [[CrossRef](#)]
24. Chen, X.; Yang, R.; Xue, Y.; Huang, M.; Ferrero, R.; Wang, Z. Deep Transfer Learning for Bearing Fault Diagnosis: A Systematic Review Since 2016. *IEEE Trans. Instrum. Meas.* **2023**, *72*, 3508221. [[CrossRef](#)]
25. Pan, S.J.; Yang, Q. A Survey on Transfer Learning. *IEEE Trans. Knowl. Data Eng.* **2010**, *22*, 1345–1359. [[CrossRef](#)]
26. Shu, X.; Shen, J.; Li, G.; Zhang, Y.; Chen, Z.; Liu, Y. A Flexible State-of-Health Prediction Scheme for Lithium-Ion Battery Packs With Long Short-Term Memory Network and Transfer Learning. *IEEE Trans. Transp. Electrif.* **2021**, *7*, 2238–2248. [[CrossRef](#)]
27. Tang, A.; Jiang, Y.; Nie, Y.; Yu, Q.; Shen, W.; Pecht, M.G. Health and lifespan prediction considering degradation patterns of lithium-ion batteries based on transferable attention neural network. *Energy* **2023**, *279*, 128137. [[CrossRef](#)]

28. Tan, Y.; Zhao, G. Transfer Learning With Long Short-Term Memory Network for State-of-Health Prediction of Lithium-Ion Batteries. *IEEE Trans. Ind. Electron.* **2020**, *67*, 8723–8731. [[CrossRef](#)]
29. Lipu, M.H.; Ansari, S.; Miah, S.; Meraj, S.T.; Hasan, K.; Shihavuddin, A.; Hannan, M.; Muttaqi, K.M.; Hussain, A. Deep learning enabled state of charge, state of health and remaining useful life estimation for smart battery management system: Methods, implementations, issues and prospects. *J. Energy Storage* **2022**, *55*, 105752. [[CrossRef](#)]
30. Schmidhuber, J.; Hochreiter, S. Long short-term memory. *Neural Comput.* **1997**, *9*, 1735–1780.
31. Zhang, Y.; Xiong, R.; He, H.; Pecht, M.G. Long Short-Term Memory Recurrent Neural Network for Remaining Useful Life Prediction of Lithium-Ion Batteries. *IEEE Trans. Veh. Technol.* **2018**, *67*, 5695–5705. [[CrossRef](#)]
32. Pan, H.; Lü, Z.; Wang, H.; Wei, H.; Chen, L. Novel battery state-of-health online estimation method using multiple health indicators and an extreme learning machine. *Energy* **2018**, *160*, 466–477. [[CrossRef](#)]
33. Yang, J.; Du, C.; Liu, W.; Wang, T.; Yan, L.; Gao, Y.; Cheng, X.; Zuo, P.; Ma, Y.; Yin, G.; et al. State-of-health estimation for satellite batteries based on the actual operating parameters—Health indicator extraction from the discharge curves and state estimation. *J. Energy Storage* **2020**, *31*, 101490. [[CrossRef](#)]
34. Cuesta-Frau, D.; Miro-Martinez, P.; Oltra-Crespo, S.; Molina-Pico, A.; Dakappa, P.H.; Mahabala, C.; Vargas, B.; Gonzalez, P. Classification of fever patterns using a single extracted entropy feature: A feasibility study based on Sample Entropy. *Math. Biosci. Eng.* **2020**, *17*, 235–249. [[CrossRef](#)] [[PubMed](#)]
35. Hu, X.; Jiang, J.; Cao, D.; Egardt, B. Battery Health Prognosis for Electric Vehicles Using Sample Entropy and Sparse Bayesian Predictive Modeling. *IEEE Trans. Ind. Electron.* **2016**, *63*, 2645–2656. [[CrossRef](#)]
36. Galatru, D.; Da Silva, C.; Romero, D.A.; Gong, Z.; Trescases, O.; Amon, C.H. Battery Health Diagnosis Approach Integrating Physics-Based Modeling with Electrochemical Impedance Spectroscopy. *Energy Technol.* **2022**, *10*, 2100942. [[CrossRef](#)]
37. Xia, Z.; Abu Qahouq, J.A. Lithium-Ion Battery Ageing Behavior Pattern Characterization and State-of-Health Estimation Using Data-Driven Method. *IEEE Access* **2021**, *9*, 98287–98304. [[CrossRef](#)]
38. Widodo, A.; Shim, M.-C.; Caesarendra, W.; Yang, B.-S. Intelligent prognostics for battery health monitoring based on sample entropy. *Expert Syst. Appl.* **2011**, *38*, 11763–11769. [[CrossRef](#)]
39. Tomčala, J. New Fast ApEn and SampEn Entropy Algorithms Implementation and Their Application to Supercomputer Power Consumption. *Entropy* **2020**, *22*, 863. [[CrossRef](#)] [[PubMed](#)]
40. Hu, X.; Li, S.; Peng, H. A comparative study of equivalent circuit models for Li-ion batteries. *J. Power Sources* **2012**, *198*, 359–367. [[CrossRef](#)]
41. Chen, L.; Lü, Z.; Lin, W.; Li, J.; Pan, H. A new state-of-health estimation method for lithium-ion batteries through the intrinsic relationship between ohmic internal resistance and capacity. *Measurement* **2018**, *116*, 586–595. [[CrossRef](#)]
42. Goel, A.; Bernstein, D.S. A Targeted Forgetting Factor for Recursive Least Squares. In Proceedings of the 2018 IEEE Conference on Decision and Control (CDC), Miami, FL, USA, 17–19 December 2018; pp. 3899–3903. [[CrossRef](#)]
43. Chu, Y.J.; Mak, C.M. A variable forgetting factor diffusion recursive least squares algorithm for distributed estimation. *Signal Process.* **2017**, *140*, 219–225. [[CrossRef](#)]
44. Wang, Q.; Wang, Z.; Zhang, L.; Liu, P.; Zhang, Z. A Novel Consistency Evaluation Method for Series-Connected Battery Systems Based on Real-World Operation Data. *IEEE Trans. Transp. Electrif.* **2021**, *7*, 437–451. [[CrossRef](#)]
45. Liang, K.; Zhang, Z.; Liu, P.; Wang, Z.; Jiang, S. Data-Driven Ohmic Resistance Estimation of Battery Packs for Electric Vehicles. *Energies* **2019**, *12*, 4772. [[CrossRef](#)]
46. Dragomiretskiy, K.; Zosso, D. Variational Mode Decomposition. *IEEE Trans. Signal Process.* **2014**, *62*, 531–544. [[CrossRef](#)]
47. Dani, K.; Hrusa, W.J.; Mizel, V.J. Lavrentiev's phenomenon for totally unconstrained variational problems in one dimension. *Nonlinear Differ. Equ. Appl. NoDEA* **2000**, *7*, 435–446. [[CrossRef](#)]
48. Tian, Y.; Lai, R.; Li, X.; Xiang, L.; Tian, J. A combined method for state-of-charge estimation for lithium-ion batteries using a long short-term memory network and an adaptive cubature Kalman filter. *Appl. Energy* **2020**, *265*, 114789. [[CrossRef](#)]
49. Elman, J.L. Finding structure in time. *Cogn. Sci.* **1990**, *14*, 179–211. [[CrossRef](#)]
50. Vennam, G.; Sahoo, A.; Ahmed, S. A survey on lithium-ion battery internal and external degradation modeling and state of health estimation. *J. Energy Storage* **2022**, *52*, 104720. [[CrossRef](#)]
51. You, G.-W.; Park, S.; Oh, D. Diagnosis of Electric Vehicle Batteries Using Recurrent Neural Networks. *IEEE Trans. Ind. Electron.* **2017**, *64*, 4885–4893. [[CrossRef](#)]
52. Zhou, W.; Lu, Q.; Zheng, Y. Review on the Selection of Health Indicator for Lithium Ion Batteries. *Machines* **2022**, *10*, 512. [[CrossRef](#)]